10

Hybrid Optoelectronic and Photovoltaic Materials based on Silicon Nanocrystals and Conjugated Polymers

Vladimir Svrcek
Research Center for Photovoltaics,
National Institute of Advanced Industrial Science and Technology (AIST),
Central 2, Umezono 1-1-1, Tsukuba, 305-8568
Japan

1. Introduction

Hybrid material, which combines advantages of both organic and inorganic materials, might offer potential for design of novel type of low cost devices with superior performance (Schneider et al., 2000; Liu et al., 2008). The large choices for the organic and inorganic structures offer the possibility to obtain materials with attractive physical and chemical properties. The ***morphology*** of hybrid material at nanoscale might lead to very different ***properties*** from crystalline solids. Particularly molecular structure polymers, conformation and orientation can have a major effect on the macroscopic properties of novel material (Coakley et la.,2003). Nanotubes are a promising subclass of nanomaterials owing unique one-dimensional geometric features that can allow engineering the polymer based material morphology at low cost. Nevertheless, nanotubes fabrication with diameter comparable with exciton diffusion lengths of polymers (~ 15 nm) is still a problem. It has to be noted that among the nanotubes with small diameter (< 5 nm), carbon-based discovered by Iijima (Iijima 1991) were the first to gain recognition in academia (Marte et al., 2001; Harris, 2002; Wang et al., 2009). Novel synthetic strategies for generating nanotubes from inorganic materials have been recently also widely investigated and developed (Tenne et al., 1992; Zhao, et al., 2004). It is believed that fiber/nanotube-polymer based arrays of material have much lower reflectance and enable fabrication of thicker devices with increased absorption compared with thin films.

One of the promising type of polymers used in variety of applications are the conjugated conductive ones (Inzelt, 2008). It has to be noted that in traditional polymers e.g. polyethylenes, the valence electrons are bound in sp^3 hybridized covalent bonds (Inzelt, 2008). Therefore sigma-bond electrons have low mobility and do not contribute to the electrical conductivity. Contrary to that conducting polymers have backbones of contiguous sp^2 hybridized carbon centers. As a result a valence electron on each center resides in a p_z orbital, which is orthogonal to the other three sigma-bonds. Then electrons within the band become more mobile particularly when it is partially emptied. This advantage combined with the mechanical properties (flexibility, toughness, malleability, etc.) make them favorable also for optoelectronic applications as an active material.

On the other hand, quantum dots, sometimes called as nanocrystals as well, are a special class of semiconductor. They range in size from 2-10 nanometers in diameter. As a result the excitons in ***quantum dots*** are confined in all three spatial dimensions (Murray, et al., 2000). Particularly, silicon nanocrystals (Si-ncs) have many advantages over the other nanocrystal materials (Canham, 1990; Hirsmman 1996). For instance, some of these materials contain toxic elements such as lead or cadmium, and others rely on elements such as indium that are in limited supply in nature. Silicon is no toxic and abundant. Newly observed phenomenon in Si-ncs - so called multiple excitons generation - favorites Si-ncs as promising material for photodetectors and solar cells (Beard,et al., 2007; Sukhovatkin et al., 2009). Namely the Si-nc can produce two or three electrons per photon of high-energy sunlight and could lead to a new type of solar cell with more than twice as efficient as nowadays used one. ***Colloidal Si-ncs*** compared to solidly embedded in matrix allow easier processibility and fabrication of device at low cost. [6] Free-standing Si-ncs and conjugated polymers blends shown be a promising optoelectronic and photovoltaic composite material (Švrček et al., 2008a; Lui et al., 2009).

In first part of this chapter we show that electrochemical etching and laser nanosecond laser processing in liquid media is suitable for preparing doped (boron and phosphorus) colloidal and surfactant free Si-ncs. Blends optoelectronic properties consisting of doped Si-ncs and two conjugated polymers (e.g. (poly(3-hexylthiophene) (P3HT) and poly[methoxy-ethylexyloxy-phenylenevinilene] (MEH PPV)) are discussed in details. It is demonstrated that such Si-ncs can be successfully used for fabrication of room temperature photoluminescent and photoconductive blends. The role of selected Si-ncs synthesis techniques on the photoelectric properties of blends is compared. We argue that the luminescence and transport properties of the blends are controlled by Si-ncs properties and could be assigned to quantum confinement of excitons in Si-ncs. We demonstrate that the transport properties of the blend can be tuned by processing conditions. The blends containing Si-ncs produced by the laser ablation clearly evidence superior photovoltaic properties due to the enhanced bulk-heterojunction surface area and improved charge transport.

The morphology of the bulk-heterojunction can be significantly affected by various fabrication parameters during the device formation. In second part of the chapter, in order to achieve an efficient performance of the bulk-heterojunction, both the size distribution and mesoscopic ordering of blend in nantubes is discussed. It is shown that a fiber- and/or vertical 1D-like order of photosensitive bulk-heterojunction gives considerable advantages over the thin film technology, because it provides larger interfacial area for efficient exciton dissociation and straight path for photogenerated carries. As a result, fibers help to avoid circuit shorts and interruption of percolation paths for carriers to their respective electrodes. In this respect, a capillary induced filtering and assembly of blends in nanoporous templates is discussed. We show that the titanium/alumina dioxide (TiO_2/Al_2O_3) nanotubes template could be suitable candidate for vertical order of photosensitive based blends.

2. Experimental methods

Colloidal and surfactant free Si-ncs with quantum confinements effects were prepared by two independent techniques. First by electrochemical etching and second by laser ablation of silicon wafer in water. For this purpose, boron-doped wafer with a resistivity of 0.5–

0.75Ocm (p-type, B concentration of $3x10^{16}cm^3$) and phosphorous-doped wafer with a resistivity of 0.5–2Ocm (n-type, P concentration $2x10^{16}cm^3$) were used. The wafers were electrochemically etched in a mixture of hydrofluoric acid with pure ethanol ($HF:C_2H_5OH$ 1:4). In order to obtain a similar size distribution of Si-ncs, a constant current density 3.2 mA/cm^2 and a constant etching time 60 min were used for the B-doped Si-ncs. In the case of P-doped Si-ncs, we kept a constant current density at $1.6mA/cm^2$. In this process, the etching time was 90 min and a halogen lamp illuminated the P-doped silicon substrate during the electrochemical etching. The B- and P-doped and red luminescent Si-ncs were harvested by mechanical scratching (Švrček et al., 2004). Second technique goes after the synthesis route of blue luminescent Si-ncs based on a water-confined nanosecond laser ablation process [Švrček et al., 2006; Švrček et al., 2009]. Particularly, the Si-ncs are prepared by nanosecond excimer pulsed laser (KrF, 245 nm 20 Hz, 20 ns). Crystalline silicon doped wafers with same characteristics as used for electrochemical etching is used for synthesis of the Si-ncs. The wafers are adhered to the bottom of a glass container and immersed in 10 ml water. The laser beam is focused onto a 1.5 mm diameter spot on the wafer surface by a lens with a focal length 25 cm. The ablation process is continued for 2 hours at room temperature and ambient pressure. Following the ablation process the aqueous solution with produced Si-ncs is left to age in ambient conditions (Švrček et al., 2009a). In order to obtain enough high Si-nc concentration for blend fabrication the process was repeated several times.

Blends consisting of red and blue luminescent Si-ncs and two conjugated polymers (poly(3-hexylthiophene) (P3HT) and poly(methoxy ethylexyloxy phenylenevinilene) (MEH PPV)) were fabricated as follow. A commercially available (ALDRICH) polymer P3HT was dissolved in chlorobenzene (12 mg of polymer in 10 g of chlorobenzene). The Si-ncs powder was mixed with polymer in order to make films. The 300 nm thin films were spun on quartz substrates. The samples were dried at 140 ˚C for 30 min in vacuum. Furthermore, we have fabricated solar cell based on the Si-ncs prepared by laser ablation and electrochemical etching. Glass substrates with an indium tin oxide (ITO) electrode were used for solar cells fabrications. The PEDOT:PSS is used as electron blocking layer and the hole collector in this structure. An alumina contact film (~100 nm) deposited on the top serves as electron collector. In order to smooth the ITO surface the poly(3,4-ethylenedioxythiophene):poly(styrene sulfonic acid (PEDOT:PSS) was deposited by spin-casting (~ 100 nm). Subsequently, the Si-ncs/P3HT solution was spin-coated on the PEDOT:PSS/ITO substrate. Then, an alumina top electrode of 100 nm was deposited on top of the active layer.by vacum evaporation. The active area of the cell was 4 mm^2.

In order to perform the alignment of the blends two types of nanotube arrays with rather same diameter were used: alumina and titanium dioxide. The nanoporous alumina membranes were fabricated by the two step anodization of 99.99% pure aluminum foil under the constant potential of 40 V in 0.3 M oxalic acid electrolyte at 5°C. The first anodization step lasted 15 h to promote spatial self-organization of nanopores. Then the thick nanoporous layer was selectively dissolved in the mixture of chromic (20 g/l) and phosphoric (66 g/L) acids leaving a highly ordered concave pattern on the surface of aluminum. The ordered concaves acted as a self-assembled mask for the nucleation of nanopores during the second anodization step. In order to perform the filtering of Si-ncs blended with an MEH-PPV polymer on the membrane was glued to an O-ring. The aluminum retained on the back side was selectively dissolved in saturated HgCl2 solution at room temperature. The barrier oxide layer was etched in 5% phosphoric acid with the

formation of a through-hole membrane (Švrček et al., 2010). All samples were carefully cleaned in distilled water and then observed in a scanning electron microscope (SEM). To perform the filtering it was necessary to decrease the viscosity of the blend by adding of 2 g of chlorobenzene into the blend solution before dropping it on the membrane. The O-ring that sealed the edge membrane did not allow the outlet of the solution (Švrček et al., 2010). The formation of Si-ncs/MEH-PPV fibers occurred when the viscosity of the Si-ncs/MEH-PPV blend dropped on the top of nanoporous alumina. The formation of the Si-ncs/MEHPPV nanofibers was confirmed by the dissolution of the alumina membrane in 5% phosphoric acid. After the dissolution, the fibrous structures were observed in SEM. In order to infiltrate the bulk-heterojunction, the TiO_2 nanotubes with rather the same inner diameters (~ 90 nm) were prepared as follows. A 99.99% pure titanium foil was anodized in 0.3 wt% solution of NH4F in ethylene glycol in a two-electrode configuration under constant potentials of 40 V at room temperature (Švrček et al., 2009b). The titanium foil served as anode and platinum mesh as the counter electrode. The transformation of amorphous as grown anodic TiO_2 into crystalline anatase was performed by annealing in air at 450 C.
The photoluminescence (PL) measurements of colloidal solutions were carried out at room temperature using fluorophotometer (Shimadzu Corporation, RF–5300PC) with excitation by Xe lamp at 300 nm for Si-ncs prepared by laser ablation and 400 nm by electrochemical etching, respectively. For the temperature dependence of the PL, a HeCd laser (325 nm) has been used. The samples were placed in the cryostat with a varying temperature from 4 to 300 K. Spectrally resolved photoconductivity was measured under illumination with monochromatic light from a Xe lamp at room temperature and N2/air atmosphere. In all cases the irradiation intensities were calibrated by a standard a-Si solar cell. A small droplet of obtained colloidal solution was deposited onto a copper grid with carbon film for high resolution transmission electron (HR-TEM) and scanning electron microscope (SEM) observations. The SEM images were done with a Hitachi SI 4800 microscope with 30 kV acceleration voltage. The HR-TEM studies were performed on a microscope with 200 kV acceleration voltage (JEOL, JEM 2010).

3. Freestanding room temperature luminescent Si-ncs

Figure 1 (a) shows the room-temperature photoluminescence (PL) spectra intensity as a function of wavelength of n- and p-type doped silicon nanocrystals (Si-ncs) excited at 325 nm prepared by electrochemical etching. We tuned the nanocrystal size distribution, the shape and the position of PL spectra by electrochemical etching conditions (Švrček et al., 2009c) and prepared freestanding Si-ncs with rather similar size distributions. This allowed as better revealing the effects of the dopands (Švrček et al., 2009c). The n-type and p-type doped freestanding Si-ncs show orange PL under at room temperature. For both types the broad PL spectra with a maximum located around 600 nm appeared. In the case of Si-ncs prepared by ns laser ablation in water aging in water is required to obtain visible PL at room temperature (Švrček et al., 2009a). After this procedure our results showed that the PL is stable and does not degrade under continuous exposure to the air or water. Fig 1(b) represents PL typical spectra of doped Si-ncs prepared by an excimer KrF laser ablation in water and aged in water for several months. Visible blue-room temperature PL is observed from both n-type doped crystalline silicon wafer (red line) and image p-type doped (black line) colloids under He:Cd laser excitation at 325 nm. The Si-ncs dispersed in colloidal

solution show blue-bands with maxima at around 420 nm. Compared to the Si-ncs made from p-type doped wafer, the PL band for n-type doped is stronger more than 2 times due to the surface passivation and presence of dopants (Lulease, et al., 2002). The origin of the broad band behavior is most likely due to multiple electronic states in Si-ncs. In both preparation methods the large size distribution results in the broadening of the PL spectra. The quantum confinement in Si-ncs with different sizes is responsible for the broad emission.

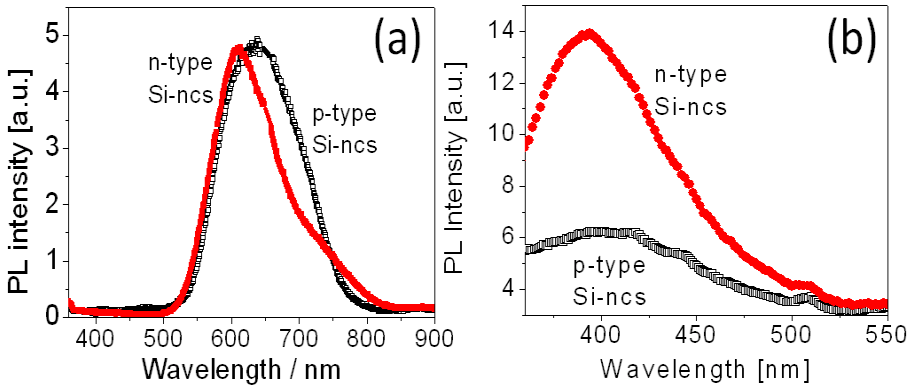

Fig. 1. (a) Room-temperature photoluminescence (PL) spectra intensity as a function of wavelength of n- and p-type doped silicon nanocrystals (Si-ncs) prepared by electrochemical etching. (b) PL spectra of doped Si-ncs prepared by an excimer KrF laser ablation in water and aged in water for 7 months

Temperature-dependent PL analysis gives an inside of the PL origins (Švrček et al., 2009a; Švrček et al., 2009c). Our results show that for Si-ncs prepared by both techniques two bands could be identify by low temperature analysis. The temperature dependence of the PL intensity for a P-doped and for a B-doped Si-ncs prepared by electrochemical etching and laser ablation showed two broad PL bands at various temperatures. For electrochemical etching the short wavelength-band locates at 500–700 nm with a maximum around 590 nm and the long-wavelengths band locates at 650–850nm with a maximum at 740 nm. In the case of laser ablation both bands are blue shifted and the maxima are centered at ~410 nm and ~525 nm, respectively. Short wavelength bands originating from delocalized carriers at the nanocrystal core with the oxide interface do not showed any temperature dependence behavior. Contrary to that, in the long wavelength band, the PL intensities of the shorter wavelengths decrease more slowly due to the state-filling effect, which results in a red shift. Figure 2 represents the shift of PL maxima as a function of temperature for Si-ncs prepared by electrochemical etching and laser ablation in water. It is supposed that the red shift is mainly attributed to the decrease in the band gap energy with temperature, which is typical for semiconductor materials due to the many possible electronic states in Si-ncs (Kovalev, et 1994; Zhuravlev et al., 1998; Garcia et al., 2003). At 4 K, the contribution from quantum confinement is distinguished quite well and one could evaluate real Si-ncs size. It is

assumed that the PL spectra with a maximum at 590 nm represent the contribution from excitons confined in nanocrystalites with a corresponding size of 2–3 nm prepared by electrochemical etching (Švrček et al., 2009c) and 1-2 nm by laser ablation (Švrček et al., 2009a).

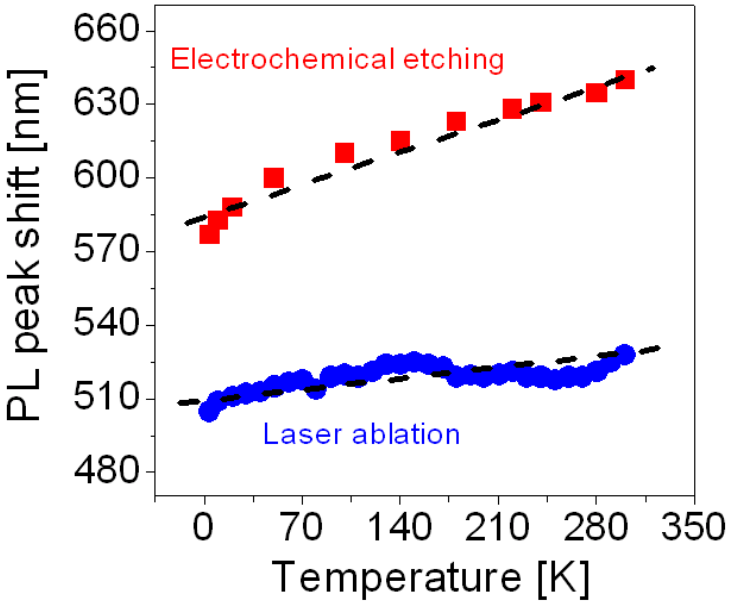

Fig. 2. Shift of PL maxima as a function of temperature for p-type doped Si-ncs prepared by electrochemical etching and laser ablation in water is shown

Photographs in Fig. 3 represent room temperature emission of Si-ncs dispersed on the quartz substrate. Photograph (a) shows the red PL of Si-ncs prepared by electrochemical etching and photograph (b) blue PL of Si-ncs fabricated by laser ablation. The Si-ncs are by HeCd laser at a wavelength of 325 nm excited. The PL emission and intensity in both cases is enough high as observed by naked eye. The wavelength of the PL maximum and that of the emission from the 525 nm band remain stable. During air exposure, oxygen penetrates near the core or on the core interface forming a Si—O—Si layer on the nanocrystal core surface. Subsequently, the Si—Si or Si—O—Si bonds become weaker or even break apart because of a larger induced stress (Ourmazd, et al., 1987). A higher number of Si-O double bonds is likely to be formed that contribute to stabilize the nanocrystal interface by terminating two dangling bonds [Herman et al., 1981). Overall, an improved surface stabilization and passivation for the dangling bonds results in a PL increase for the large wavelength bands. It has been reported that the quantum yield of blue PL colloidal Si-ncs prepared by other techniques decreases during oxidation since a recombination channel for the Si-ncs and the expected PL due to quantum confined excitons is quenched (Jurbergs et al., 2006).

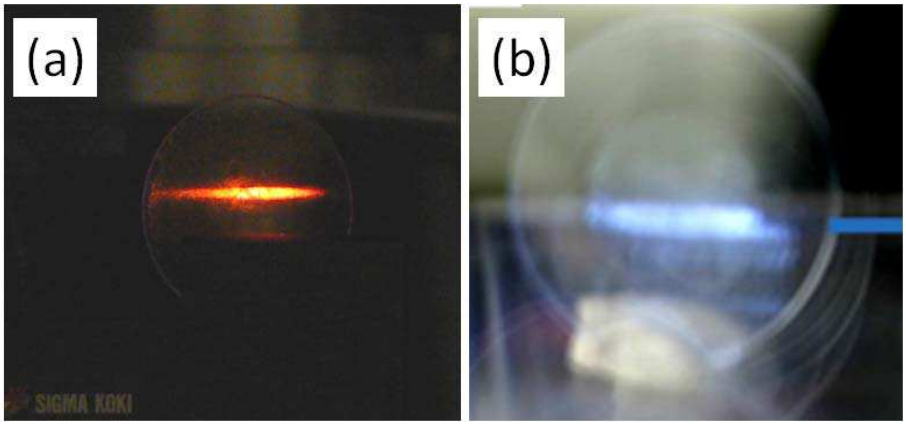

Fig. 3. Photographs of red-orange and blue light emission from Si-ncs dispersed on quartz prepared (a) by electrochemical etching and (b) by laser ablation in water. Si-ncs were excited by a He:Cd laser at 325 nm at room temperature

Systematic studies of high-resolution transmission electron microscopy (HR-TEM) observations showed that such powder contains both single Si-ncs and Si-ncs micrograins (Švrček et al., 2004). Figure 4a shows TEM images of Si-ncs prepared by electrochemical etching. While also the Si-ncs micrograins consist of many nanocrystals (ranging from about 2 to 6 nm) interconnected and kept together by amorphous tissue particles with size several tenths nanometers are observed. Figure 4 (b) represents a typical TEM image of Si-ncs particles prepared by laser ablation processing in water by ns KrF laser. Detailed TEM (APL) revealed that spherical particles with average size of 40 nm containing the Si-ncs with size ~ 1-3 nm. Independently to TEM also Raman spectra, XRD structural analyses of particles prepared by two independent techniques confirm the presence of Si-ncs with the crystalline silicon diamond-like structure (Švrček et al., 2004), indeed, smaller sized Si-ncs were clearly achieved by laser ablation in liquid media (Švrček et al., 2006).

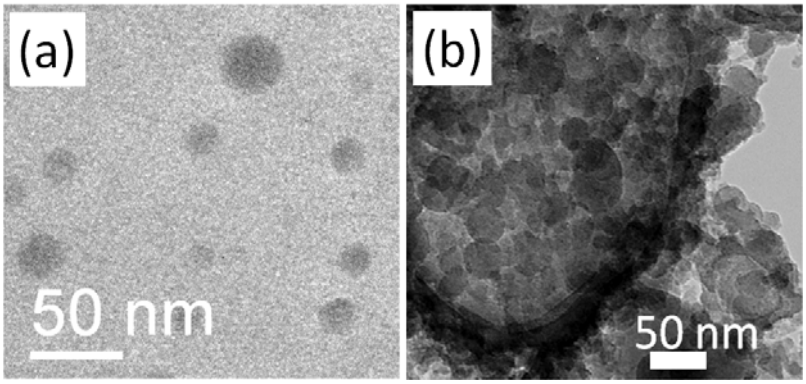

Fig. 4. Transmition electron microscopy (TEM) images of silicon nanocrystals (Si-ncs) prepared (a) by electrochemical etching and (b) by nanosecond excimer KrF laser ablation in water

4. Si-ncs and conjugated polymer s based composites

We have shown recently that freestanding Si-ncs allows the fabrication of hybrid organic-inorganic composites with a high Si–nc with nonlinear optical properties (Švrček et al., 2002; Švrček et al., 2004). In addition, polymers properties could be flexible tuned for example by doping or type of polymer. On the other hand the transparency of silicon dioxide based polymer allows preparing the Si-ncs by nanosecond laser ablation of the Si target in this type of polymer (Švrček et al., 2008b). The confinement of laser generated enhances the formation of Si-nc and the silicon-dioxide-based SOG inhibited Si-nc aggregation compared to the case of laser ablation in water. The silicon-dioxide-based SOG during the solidification process accelerates nanocrystal surface oxidation resulting in visible room temperature PL with a maximum located at ~ 400 nm. The solidification of Si-nc in SOG solution enabled the formation of self-supporting films with well-defined Si-nc concentrations that could be simply varied by laser fluence (Švrček et al., 2008b).
As the conductivity is crucial for optoelectronic application (e.g. LED), however, the SOG polymers shows very low transport properties. Contrary to that conjugated polymers can allow to overcome the problem. Between them (poly[2-methoxy, 5-(2-ethylhexoxy)-1,4-phenylene vinylene]) *MEH-PPV* and P3HT are particularly well studied and already applied for optoelectronics and photovoltaics device development. As reprted elsewhere, a series of commercial organic/inorganic materials were blended into those polymers and used for instance as electron acceptors in the bulk heterojunction structure based devices (Yue et al., 2010).

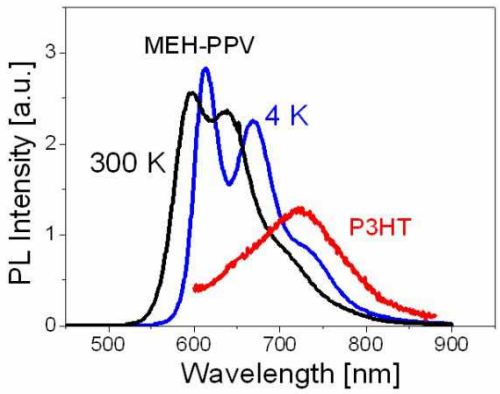

Fig. 5. Photoluminescence (PL) spectra taken at 4 and 300 K of pure MEH-PPV polymer under the same excitation conditions, for comparison. Red line represents typical PL spectrum for P3HT polymer at room temperature

Figure 5 shows typical PL spectra of our used conjugated polymer. In figure 5 blue line show PL spectra taken at 4 and black one at 300 K of pure MEH-PPV polymer, respectively. In this case three characteristic PL peaks, correlating with a zero phonon transition and two phonon replicas are detected. Red line represents the PL spectrum for P3HT polymer at room temperature and is shown for comparison. After Si-ncs introduction within both polymers high absorption of both polymers doesn't allow simple visualization of Si-ncs. The

question arisen whether after blending we could see Si-ncs contribution to overall optical properties of such hybrid material. Figure 6 presents' typical PL spectra of the Si-ncs prepared by electrochemical etching and blended in (a) MEH-PPV (b) P3HT conjugated polymers. Figure 6(c) shows the spectra of the Si-ncs prepared by laser ablation in water and blended in P3HT polymer. All spectra are taken under laser c.w. laser excitation (at 325 nm) at 4 and 300 K, respectively. For both polymers based on both doped Si-ncs and prepared by different technique a similar PL emission behavior was observed. Fig 6d represents a summary of the PL peaks position of the blends made of Si-ncs fabricated by electrochemical etching (red circles) and laser ablation (blue squares) as a function of the temperature. Peak position of the pure P3HT polymer film only is shown for comparison (black symbols). We note that the PL behavior of both polymers as a function of the temperature is rather the same and a clear blue shift of ~60 meV is recorded in the same temperature range (4–300 K). Contrary to the pure polymers, the PL spectra are shifted in the opposite direction as a function of temperature. As the temperature was increased in the range from 4 to 300 K the PL intensity and the band shifts varied monotonically. Namely the PL intensities of the shorter wavelengths decreased more slowly due to the state filling effect. Delocalized carriers at the nanocrystal–polymer (P3HT and MEH-PPV) interface also contributed to Si-ncs emission. It is supposed that the red shift is mainly attributable to a decrease in band gap energy with temperature, typical of semiconductor materials (Švrček et al., 2009c).

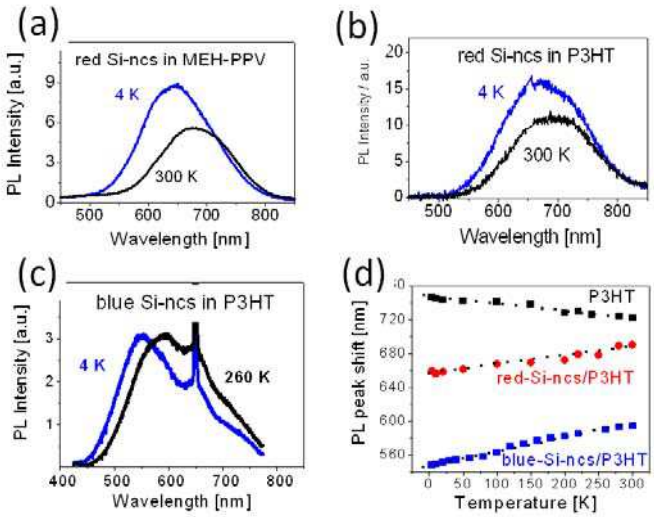

Fig. 6. Typical photoluminescence (PL) spectra of the Si-ncs prepared by electrochemical etching and blended in (a) MEH-PPV (b) P3HT conjugated polymers. (c) The spectra of the Si-ncs prepared by laser ablation in water and blended in P3HT polymer. The spectra are taken under laser cw laser excitation (at 325 nm) at 4 and 300 K, respectively. (d) Summary of the PL peaks position of the blends made of Si-ncs fabricated by electrochemical etching (red circles) and laser ablation (blue squares) as a function of the temperature are shown. Peak position of the pure P3HT polymer film only is shown for comparison (black symbols)

We show that a top-down by electrochemical etching and bottom up by laser ablation are suitable approaches for preparing doped (boron and phosphorus) freestanding and surfactant-free Si-ncs. Then they can be successfully used for the fabrication of room temperature photoluminescent and photosensitive blends based on MEHPPV or P3HT copolymer. We argue that the PL properties of the blends are controlled by the Si-ncs properties and could be assigned to quantum confinement of excitons in nanocrystalites. Generally it is accepted that when a nanocrystal is capped by an organic layer (ligands) the excitation transfer is dominated by the Förster mechanism and attributed to a dipole-dipole coupling process [Förster, 1959; Chang, et al., 2004). In our case, we prepared the Si-ncs surface without any surfactant (i.e. ligands), which limits dipole-dipole coupling. In this case the acceptor-donor pairs are in close distance, the excitation transfer is dominated by the Dexter mechanism, which is a charge exchange process (Dexter, 1953; Greenham, et al., 1996). We assume that in our case the donor and acceptors are in direct contact or at least in van der Waals contact. The Dexter energy transfer rate (R_{ET}) between a donor-acceptor pair at a distance (*d)* can be written as follow

$$R_{ET}(d) = \frac{2\pi}{\hbar\Psi^2}\int P_D(E)A_A(E)dE \tag{1}$$

where $P_D(E)$ is donor emission and $A_A(E)$ is acceptor absorption. The excitation-transfer energy from the respective polymer to nanocrystal leads to a red shift of the blends PL emission. Even the Forester mechanism cannot be completely ruled out it is assumed that after the Dexter-like energy transfer of the PL band can be attributed mainly to zero-phonon electron–hole recombination in Si-ncs due to a strong enhancement of the quantum confinement effect.

5. Bulk-heterojunction and photovoltaic properties of Si-ncs/P3HT polymer composites

Figure 7(a) shows an energy band diagram of the conjugated polymer and Si-ncs. Also optical measurements suggested that electronic interaction between both types of conjugated polymers occurred. As a result the blending of Si-ncs in both conjugated polymers led to the establishment of a bulk-heterojunction between the Si-ncs and polymer. It is assumed that a fraction of the excitons dissociated at the Si-nc/polymer interface (Švrček et al., 2008b, Švrček et al., 2009c). The HOMO for P3HT and MEH-PPV was 5 eV under vacuum, with the lowest unoccupied molecular orbital (LUMO) at 3 eV. Although the exact work function for Si-ncs is not yet known, it is expected that the value will not be significantly different from the position of the conduction band of bulk silicon (4.1 eV). The optical band gap of the silicon nanocrystallites used is 2 eV in the case of electrochemically etched Si-ncs and 2.9 eV prepared by laser ablation in water, respectively. Thus allow proper bands adjustment and e–h separation in both cases. The different electron affinities and ionization potentials provided a driving force for dissociation when the excitons were generated under irradiation. Compared to MEH-PPV photoconductive response is more important in the case of the lamella like P3HT (Švrček et al., 2009c). This mainly due to a simplify transport of photogenerated carrier in P3HT (Švrček et al., 2009c). In order to determinate the influence of the Si-ncs size on photocurrent generation we have fabricated device based on Si-ncs prepared by laser ablation and electrochemical etching. Fig 7(b)

represents schematic structure of Si-ncs/P3HT blend based device. Glass substrate with an ITO electrode was used and an alumina top electrode was deposited on top of Si-ncs/P3HT active layer.

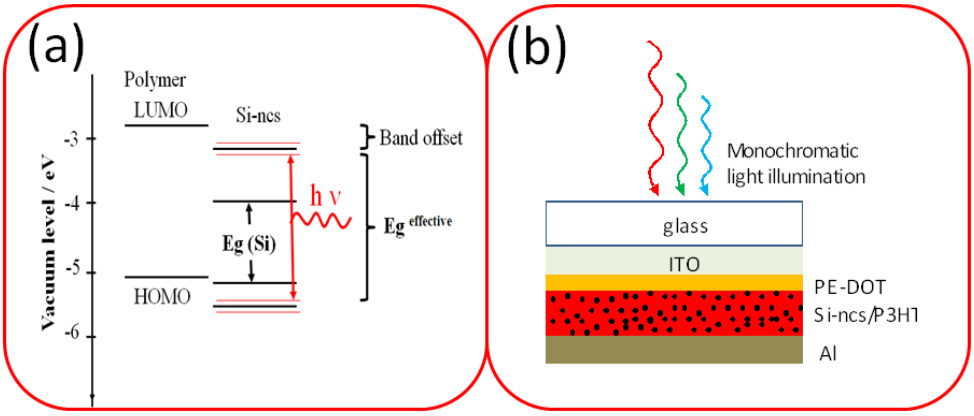

Fig. 7. (a) Energy band diagram of the MEH-PPV polymer and Si-ncs. (b) Schematic structure of Si-ncs/polymer blend based device

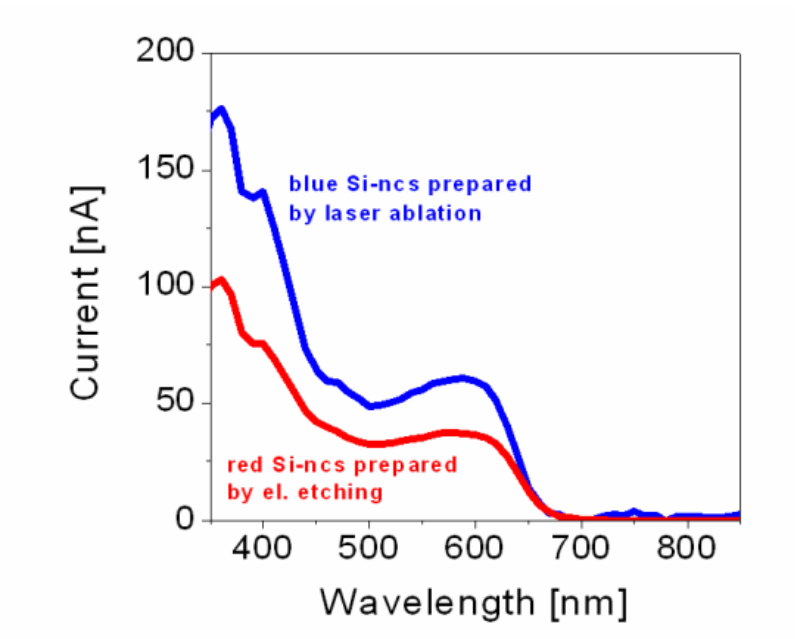

Fig. 8. Photocurrent generation in the Si-ncs/P3HT blends (~38 wt. % concentration of Si-ncs) synthesized by two methods. Red line represents blend with the Si-ncs prepared by electrochemical etching and the blue line by nanosecond laser ablation in water

Figure 8 compares photocurrent generation as a function of the wavelength for blends containing of the Si-ncs blended at ~ 38 wt. % concentration. Red line corresponds to the Si-ncs prepared by electrochemical etching and blue line to Si-ncs synthesized by laser ablation in water. A more important increase in photoconductivity is noticed for the films containing of the blue-luminescent nanocrystals prepared by laser ablation. Similar to disccused above (Švrček et al., 2009c), it is believed that large fraction of the excitons dissociates at Si-nc/polymer interface. Since Si-ncs prepared by laser ablation are smaller in radius (1.5-3 nm) the bulk-heterojunction inteface for exciton dissociation is larger. Then the exciton separation rate is superior to the blend fabricated from the electrochemically etched Si-ncs where the radius is 3-5 nm in average.

6. Filtering and ordering of Si-ncs/co-polymers hybrid composites in nanotubes

It is believed that arrangement of flexible Si-ncs based blends in a form of long nanofibers could resolve multiple problems. It is supposed that the fibrous-like structure will lead to an alignment of Si-nc polymer chains and allow the formation of thicker devices. The nanofiber perpendicular orientation might improve charge collection efficiency through the creation of uninterrupted percolation paths for photogenerated carriers generated by bulk-heterojunction. Noteworthy to say that the nanofiber structure provides a larger interfacial area and has a much lower reflectance compared with the thin films. Several nanotubular architectures have been investigated for potential enhancement of electron percolation pathways in bulk-heterojunction (Coakley et la.,2003). We believe that the nanoporous anodic alumina and TiO_2 are the most feasible large-scale templates that can be used for blend alignment. Furthermore, the size distribution of freestanding Si-ncs can be improved by filtering across the anodic alumina membrane (Švrček et al., 2010). The filtering through the alumina membrane can be used to narrow the size distribution of Si-ncs blended with MEHPPV polymer as well. Figure 9 (a) presents typical top-view SEM images of the nanoporous membrane with an average diameter of 85 nm. The SEM image shows a well-ordered hexagonal packing of the alumina nanopores with a uniform pore size distribution. The high surface energy and O-ring that seal the edges of the membrane kept the liquid on the top of the alumina membrane within the O-ring (Švrček et al., 2010). Then, induced capillary forces from the bottom establish the liquid flow through the opened alumina membrane.

Wettability is another important factor, which contributes to the establishing the flow across one membrane (Švrček et al., 2010). The Young–Laplace equation is commonly used to describe the pressure drop across (Marle, 1981). Once the flow is established, the hydrodynamic flow can be described by the Hagen–Poiseuille equation (Blom, et al., 1996, Švrček et al., 2009c). In this case we deal with the large diameter of pores (Švrček et al., 2010), the flow rate (R) across the alumina nanoporous membrane can be written as

$$R = \frac{\pi d^4}{128\eta}\left(\frac{P}{L}\right) \tag{2}$$

where P is the pressure drop across the pore, d is the pore diameter, η is the solvent viscosity, and L is the membrane thickness. It has to be noted that we achieved the capillary induced wetting of the nanopores when the viscosity of the Si-ncs/MEH-PPV blend

dropped on top of nanoporous alumina was high enough to prevent free flow of the blend through the membrane. Compared to TiO_2 advantageous of alumina membrane is that it is easily to be dissolved without dissolution of blend. After dissolution of the membrane in weak 5 wt % phosphoric acid, we could observe the presence of a Si-ncs/MEH-PPV nanofibrous blend. Figure 10 shows typical SEM image of the Si-ncs/MEH-PPV nanofibers after dissolution of the nanoporous alumina membrane. Our observation showed the formation of randomly oriented long fibers only, without the presence of nanotubes. The diameter of the fibers corresponds to the diameter of the alumina nanopores ~80 nm. The wetting phenomena and the presence of Si-ncs in the polymer did not allow formation of nanotubes. However, the nanoporous alumina membrane was quite thick 50 μm and the perpendicularly ordered fibers collapsed. The EDS spectra reveal less oxygen in the blend when after filtering (Švrček et al., 2010). It is supposed that an improvement of both the Si-nc size distribution and the blend morphology limits the oxygen diffusion into the blend. It is well known that oxygen is one of the main factors that lead to the degradation of conjugated polymer-based devices (Scott, et al., 1996]). As this processing can be performed at room temperature it might find application in the future development of new types of optoelectronic and photovoltaic devices.

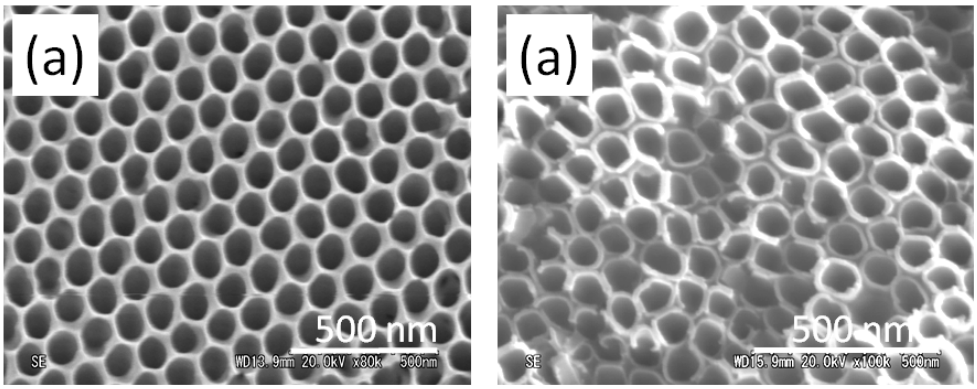

Fig. 9. (a) Top-view SEM images of the nanoporous membrane with average diameter of ~85 nm used for experiments. (b) SEM image of the nanotubular TiO_2 template with diameter of ~90 nm used for vertical order of Si-ncs conjugated polymer based blend

Previous experiments confirmed that the blend can flow through pores with such a diameter. Following of those experiments we have used TiO_2 nanotube template with rather same diameter that the same time serves as an electrode for hybrid device. The morphology of the TiO_2 nanotube with average diameters of 90 nm after thermal treatment is shown in Fig. 9 (b). The transformation of amorphous TiO_2 into crystalline anatase was confirmed by XRD measurements and after the annealing process two most important TiO_2 anatase peaks corresponding to (101) and (200) orientations were clearly recorded (Švrček et al., 2009b). It is observed that infiltration of photosensitive Si-ncs/P3HT blend in the TiO_2 nanotubes results in increase in the photovoltage generation. One can expected that the alignment of Si-ncs/P3HT bulk-heterojunction within TiO_2 nanotubes, which are perpendicular to the contact, will facilitates charge transfer along the nanotubes and reduces losses incurred by charge hopping across the Si-ncs/P3HT blend (Švrček et al., 2009b). Figure 11 (a) shows a

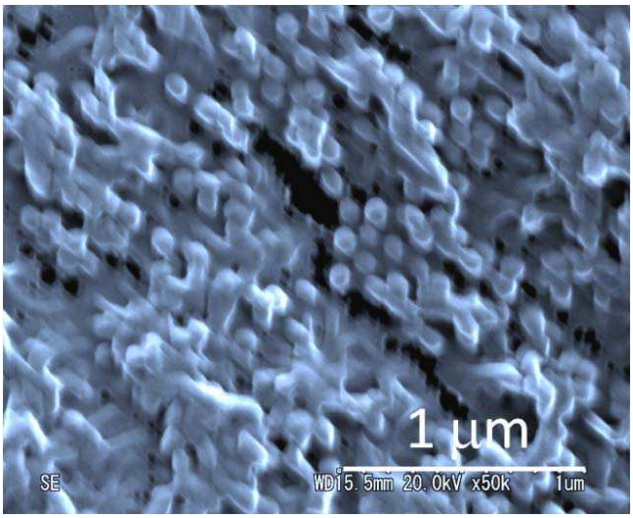

Fig. 10. Scanning electron microscopy image of the Si-ncs/MEH-PPV nanofibers after dissolution of the nanoporous alumina membrane

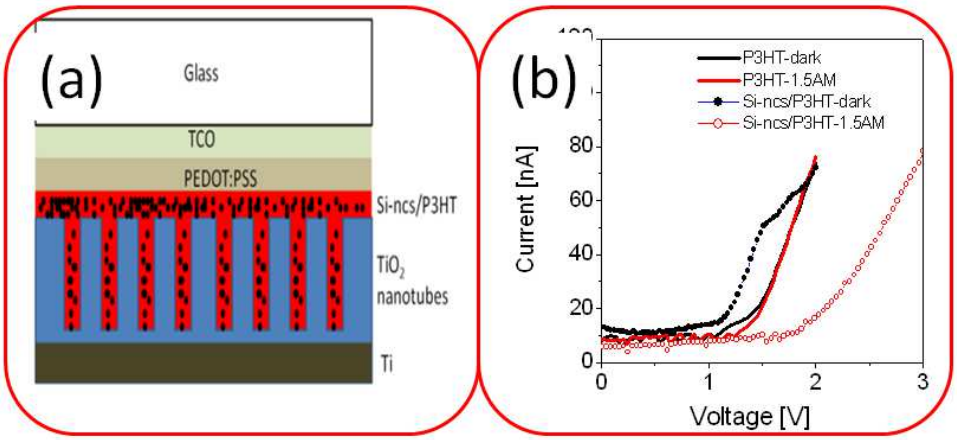

Fig. 11. (a) Schematic sketch of the structure for ordering of Si-ncs/P3HT bulk-heterojunction in TiO_2 nanotube arrays. (b) The current voltage (I–V) characteristics from the pure P3HT polymer and Si-ncs/P3HT blend aligned in within TiO_2 nanotube arrays with the diameters of 90 nm in dark and under illumination AM1.5

schematic sketch of the structure used for alignment of Si-ncs/P3HT bulk heterojunction. The corresponding I–V characteristics of Si-ncs/P3HT heterojunction in vertical configuration in the dark and under illumination at AM1.5 are compared in Fig. 11 (b). The I–V characteristics for P3HT polymer only and Si-nc/P3HT based blend show a p–i–n behavior. However, superior open voltage and ratio between the photo- and dark-

conductivity are observed in the case of infiltration of the blend into TiO_2 nanotubes (symbols in Fig. 11 (b)). The photovoltage generation in the bulk-heterojunction most likely results in increase in open circuit voltage. The presence of the Si-ncs in polymer makes the blend to be more semiconductor rather than an insulator; therefore, a high-voltage open-circuit can be partially explained by assuming a Schottky barrier at the Si-ncs/P3HT/PEDOT:PSS interface. The fiber-like geometry provides larger interfacial area, which results in enhanced exciton dissociation. The nanofiber morphology of the blend embedded into nanotubular templates contributed to high open-circuit voltage.

7. Conclusion

We showed that electrochemical etching and nanosecond laser ablation in water are suitable techniques for preparing freestanding and surfactant-free Si-ncs with quantum confinements effects. It is demonstrated that such Si-ncs can be successfully used for the fabrication of room temperature photoluminescent and photosensitive hybrid materials. The materials consisting of Si-ncs with rather different energy band gaps and conjugated polymers (poly(3-hexylthiophene) (P3HT) and poly(methoxy ethylexyloxy phenylenevinilene) (MEH PPV)) with rather similar energy band gaps were fabricated. We argue that the luminescence and transport properties of the blends can be controlled by the Si-ncs properties and could be assigned to quantum confinement of excitons in nanocrystalites. The difference in electron affinity and ionization potential between nanocrystals and polymer leads to bulk-heterojunction formation and excitons desociation. An enhanced photovoltaic effect has been achieved by blending of Si-ncs prepared by laser ablation. The device performances have been improved through enhanced bulk-heterojunction interface area and charge transport. Next, we showed that the nanotube arrays can be efficient for a vertical 1D-like order of photosensitive hybrid material. An arrangement of the Si-ncs/P3HT bulk-heterojunction within ordered Al_2O_3/TiO_2 nanotubes prepared perpendicular to the contact has been shown. It is believed that the Si-ncs non-toxicity, easy integration into well-established silicon technologies and polymer flexibility might bring considerable benefit for hybrid optoelectronic and photovoltaic device development. Needless to mention that the blend flexibility might allow easy and cost effective design new types of nanostructures for enhancement device properties.

8. Acknowledgements

This study was also partially supported by Industrial Technology Research Grant Program from the New Energy and Industrial Technology Development Organization (NEDO) of Japan.

9. References

Canham, L. T. (1990), Silicon Quantum Wire Fabrication by Electrochemical and Chemical Dissolution of Wafer, *Appl. Phys. Lett.* 57, pp.1046-1048.

Beard, M.C.; Knutsen, K.P.; Yu, P.; Luther, J.M.; Song, Q.; Metzger, W.K.; Ellingson, R.J.; Nozik, A.J., (2007), Multiple Exciton Generation in Colloidal Silicon Nanocrystals , *Nano Lett. 7, pp.* 2506-2512.

Blom, P. W. M.; De Jong, M. J. M. ; Vleggaar, J. J. M. (1996), Electron and hole transport in poly(*p*-phenylene vinylene) devices, *Appl. Phys. Lett.*, 68 pp.3308(1-3).

Chang, T. W. F.; Musikhin, S.; Bakueva, L.; Levina, L.; Hines, M.A.; Cyr, P.; Sargent, E.H.; (2004), Efficient excitation transfer from polymer to nanocrystals, *Appl. Phys. Lett.* 84, pp. 4295-4298.

Coakley, K.M.; Liu, Y.X.; McGehee, M.D.; Frindell, K.L.; Stucky, G.D. (2003), Infiltrating semiconducting polymers into self-assembled mesoporous titania films for photovoltaic applications, *Adv. Funct. Mater.* 13, pp. 301-316 .

Dexter, D.L., (1953), A Theory of Sensitized Luminescence in Solids *J. Chem. Phys.* 21, pp. 836-851.

Förster,T., (1959), 10th Spiers Memorial Lecture. Transfer mechanisms of electronic excitation *Discuss. Farraday Soc.* 27, pp. 7-17.

Garcia, C.; Garrido, B.; Pellegrino, P.; Ferre, R.; Moreno, J.A.; Morante, J. R.; Pavesi, L.; Cazzanelli, M., (2003), Size dependence of lifetime and absorption cross section of Si nanocrystals embedded in SiO2, *Appl. Phys. Lett.* 82, pp. 1595 -1598.

Greenham, N. ; Peng, X.; Alivisatos, P. (1996), Charge separation and transport in conjugated-polymer/semiconductor-nanocrystal composites studied by photoluminescence quenching and photoconductivity, *Phys. Rev. B* 54, pp. 17628-17637.

Harris, P.F.J. (2002). *Carbon nanotubes and related structures* (1st ed.). Cambridge University Press. pp. 213–32

Herman. F.; Kasowski, R. V., (1981), Electronic structure of defects at Si/SiO_2 interfaces, *J. Vac. Sci. Technol.* 19, pp. 395-401.

Hirsmman, K. D.; Tsybeskov, L.; Duttagupta, S. P.; Fauchet, P. M. , (1996), Silicon-based visible light-emitting devices integrated into microelectronic circuits, *Nature* 384, pp. 338-341.

Inzelt, G.; (2008). *Conducting Polymers* A New Era in Electrochemistry. *Springer. pp. 265–269.*

Iijima, S. (1991). Helical microtubules of graphitic carbon, *Nature,* 354, pp. 56-58.

Jurbergs, D.; Rogojina, E.; Mangolini, L.; Kortshagen, U., (2006), Silicon Nanocrystals with Ensemble QuantumYields exceeding 60%, *Appl. Phys. Lett.* 88, pp.233116 -233119.

Kovalev, D. I.; Yaroshetzkii, I. D.; Muschik, T.; Petrovakoch, V. F.; Koch P., (1994), Fast and slow visible luminescence bands of oxidized porous Si, *Appl. Phys. Lett.* 64, pp.214 - 217.

Lulease, J.; Fujii, M.; Mimura, A.; Hayashi, S., (2002) *Phys. Rev. Lett.* 89 pp.296805-.296809.

Liu, J.L.; Yan, B.; (2008), Molecular Construction and Photophysical Properties of Luminescent Covalently Bonded Lanthanide Hybrid Materials Obtained by Grafting Organic Ligands Containing 1,2,4-Triazole on Silica by Mercapto Modification, *J. Phys. Chem. C* 112, pp. 14168-14178.

Lui, C., Holman, Z., Kortshagen, U., (2009), Hybrid Solar Cells from P3HT and Silicon Nanocrystals , *Nano Lett.* 9, pp. 449-452.

Marle, C. M. (1981), *Multiphase Flow in Porous Media*, Gulf, Houston, TX .

Martel, R.; Derycke, V.; Lavoie, C.; Appenzeller, J.; Chan, K. K.; Tersoff, J.; Avouris, Ph. (2001), Ambipolar Electrical Transport in Semiconducting Single-Wall Carbon Nanotubes, *Physical Review Letters* 87: pp. 256805-256809.

Murray, C.B.; Kagan, C.R.; Bawendi, M. G. (2000), Synthesis and Characterization of Monodisperse Nanocrystals and Close-Packed Nanocrystal Assemblies, *Annual Review of Materials Research* 30 (1): pp. 545–610.

Ourmazd, A.; Taylor, D. W.; Rentschler, J.A.; Bevk, J. (1987), Si→SiO_2 transformation: Interfacial structure and mechanism," *Phys. Rev. Lett.* 59, pp. 213-216.

Scott, J. C. ; Kaufman, J. H. ; Brock, P. J. ; DiPietro, R. ; Salem, J.; Goitia, J. A.; (1996), Degradation and failure of MEH-PPV light-emitting diodes, *J. Appl. Phys.*, 79, pp. 2745-2752.

Schneider, M.; Muller, K.,; (2000), Hybrid Materials Doped with Covalently Bound Perylene Dyes through the Sol−Gel Process , *Chem. Mater.* 12 , pp. 352-362.

Sukhovatkin, V; Hinds, S.: Brzozowski, L.; Sargent, E.H.; (2009), Colloidal Quantum-Dot Photodetectors Exploiting Multiexciton Generation, *Science* 324 *pp.* 1542-1544.

Švrček, V.; Pelant, I.; Chvojka, T.; Valenta, J.; Dian, J.; Rehspringer, J.-L.; Gilliot, P.; Ohlmann, D.; Crégut, O.; Hönerlage, B., (2002), Photoluminescence properties of sol-gel derived SiO_2 films doped with porous silicon, *Materials Science & Engineering C* 19, pp.233-238.

Švrček, V.; Slaoui, A.; Muller, J.-C. (2004), Ex-situ prepared Si nanocrystals: Their elaboration and characterization in embedded silica glass, *J. Appl. Phys.* 95, pp.3158-3164.

Švrček, V. Sasaki, T.; Shimizu, Y.; Koshizaki, N., (2006), Blue luminescent silicon nanocrystals prepared by ns pulsed laser ablation in water, *Appl. Phys. Lett.*, 89, pp.213113(1-3).

Švrček, V.; Fujiwara, H.; Kondo M.; (2008a), Improved transport and photo-stability of poly[methoxy-ethylexyloxy-phenylenevinilene] polymer thin films by boron doped freestanding silicon nanocrystals, *Appl. Phys. Lett.* 92, p.143301(1-3).

Švrček, V.; Sasaki, T.; Shimizu, Y.; Koshizaki, N.; (2008b), Blue luminescent silicon nanocrystals prepared by ns laser ablation and stabilized in electronically compatible spin on glasses, *J. Appl. Phys.,* 103, pp.023101-023108.

Švrček, V.; Mariotti, D.; Kondo, M.; (2009a), Ambient-stable blue luminescent silicon nanocrystals prepared by nanosecond-pulsed laser ablation in water, *Optics Express*, 17 pp. 520-527.

Švrček, V.; Turkevych, I.; Kondo, M.; (2009b) Photoelectric properties of silicon nanocrystals/P3HT bulk-heterojunction ordered in titanium dioxide nanotube arrays, *Nanoscale Research Letters*, 4 pp.1389-1395.

Švrček, V.; Fujiwara, H.; M. Kondo, M.; (2009c) Luminsecent Properties of doped freestanding silicon nanocrystals embedded in MEH-PPV, *Solar Energy Materials & Solar Cells*, 93, pp. 774-780.

Švrček, V.; Fujiwara, H.; Kondo, M.; (2009c) Top-down silicon nanocrystals and a conjugated polymer-based bulk heterojunction : Optoelectronic and photovoltaic applications, *Acta Materialia* 57 pp.5986-5997.

Švrček. V; Turkevych, K.; Kondo, M.; (2010) Filtering and assembly of Si nanocrystals/conjugated polymers blend with reduced oxygen penetration, *Journal of the Electrochemical Society* 157 (9) pp. K194-K200.

Tenne R, Margulis L, Genut M, Hodes G (1992), Polyhedral and cylindrical structures of tungsten disulphide, *Nature* 360 (6403): pp. 444–446.

Yue, D.; Bai, X.; Zhao,S.; Miao,X.; Li, M.; Dong, J.; Ibrahim,K.; Wang, J.; Zhao,Y.; Yuan, H.; Xing, G.; Sun, B.; (2010), First Endohedral Metallofullerene-Containing Polymer:

Preparation and Characterization of Gd@C_{82}-Polystyrene, *The Journal of Physical Chemistry C 114* (17), pp. 7631-7636.

Zhao, X.; Liu, Y.; Inoue, S.; Suzuki, T.; Jones, R. O.; Andol, Y. (2004), Smallest Carbon Nanotube is 3 Å in Diameter, *Physical Review Letters* 92 (12) pp. 125502-125506.

Zhuravlev, K. S.; Gilinsky, A.M.; Kobitsky, A.Y., (1998), Mechanism of photoluminescence of Si nanocrystals fabricated in a SiO_2 matrix, *Appl. Phys. Lett.* 73, pp.2962-2965.

Wang, X.; Li, Q.; Xie, J.; Jin, Z.; Wang, J.; Li, Y.; Jiang, K.; Fan, S. (2009), Fabrication of Ultralong and Electrically Uniform Single-Walled Carbon Nanotubes on Clean Substrates, *Nano Letters* 9 (9): pp. 3137–3141

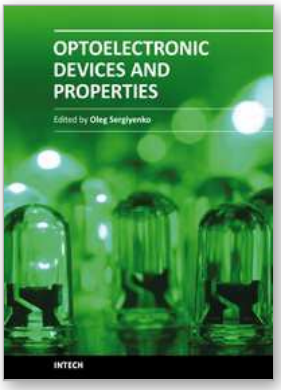

Optoelectronic Devices and Properties

Edited by Prof. Oleg Sergiyenko

ISBN 978-953-307-204-3
Hard cover, 660 pages
Publisher InTech
Published online 19, April, 2011
Published in print edition April, 2011

Optoelectronic devices impact many areas of society, from simple household appliances and multimedia systems to communications, computing, spatial scanning, optical monitoring, 3D measurements and medical instruments. This is the most complete book about optoelectromechanic systems and semiconductor optoelectronic devices; it provides an accessible, well-organized overview of optoelectronic devices and properties that emphasizes basic principles.

How to reference

In order to correctly reference this scholarly work, feel free to copy and paste the following:

Vladimir Svrcek (2011). Hybrid Optoelectronic and Photovoltaic Materials based on Silicon Nanocrystals and Conjugated Polymers, Optoelectronic Devices and Properties, Prof. Oleg Sergiyenko (Ed.), ISBN: 978-953-307-204-3, InTech, Available from: http://www.intechopen.com/books/optoelectronic-devices-and-properties/hybrid-optoelectronic-and-photovoltaic-materials-based-on-silicon-nanocrystals-and-conjugated-polyme

INTECH
open science | open minds

InTech Europe
University Campus STeP Ri
Slavka Krautzeka 83/A
51000 Rijeka, Croatia
Phone: +385 (51) 770 447
Fax: +385 (51) 686 166
www.intechopen.com

InTech China
Unit 405, Office Block, Hotel Equatorial Shanghai
No.65, Yan An Road (West), Shanghai, 200040, China
中国上海市延安西路65号上海国际贵都大饭店办公楼405单元
Phone: +86-21-62489820
Fax: +86-21-62489821